Advances in Science and Technology Research Journal

Advances in Science and Technology Research Journal, 2025, 19(6), 275–290
https://doi.org/10.12913/22998624/202753
ISSN 2299-8624, License CC-BY 4.0

Received: 2025.01.03
Accepted: 2025.04.15
Published: 2025.05.01

Determining a damping coefficient by using a microelectromechanical systems accelerometer for finite element method simulation purposes on a discrete damper example

Leszek Flis[1*], Grzegorz Szwoch[2], Piotr Krawczyk[1]

[1] Department of Mechanical Engineering, Polish Naval Academy of the Heroes of Westerplatte, ul. Śmidowicza 69, Gdynia, Poland
[2] Department of Mechanical Engineering, Gdansk University of Technology, ul. Gabriela Narutowicza 11/12, Gdańsk, Poland
* Corresponding author's e-mail: l.flis@amw.gdynia.pl

ABSTRACT

The paper presents a fast method for determining the damping coefficient using a microelectromechanical systems (MEMS) accelerometer, demonstrated on the example of a discrete damper element used in FEM simulations. The primary focus is on addressing a critical gap in current FEM modelling – damping is traditionally expressed as a percentage without a direct physical correlation in SI units. Additionally, there is a lack of efficient methods for quickly estimating damping in equipment that can be modelled as discrete elements. A methodology is designed specifically for one-dimensional discrete elements such as springs and dampers in FEM simulations. A key advantage of this approach is its reliance on simple, readily available measurement equipment, allowing for easy reproducibility of results without the need for complex laboratory apparatus, where repeatability is often difficult or impossible to achieve outside the laboratory, whereas the presented method offers such capabilities.

Keywords: damping, acceleration, vibrations, MEMS, LS-Dyna.

INTRODUCTION

Damping plays a crucial role in FEM-based structural dynamics and vibration analysis. However, numerical methods used in FEM simulations rely exclusively on Rayleigh damping Equation 1, which lacks a direct physical justification [1]

$$[C] = \alpha[M] + \beta[K] \tag{1}$$

where: $[C]$ is the damping matrix of the physical system, $[M]$ is the mass matrix, $[K]$ is the stiffness matrix, and α and β are constants.

It can be challenging to guess meaningful values for the Rayleigh damping coefficients α and β, especially for systems with single degrees of freedom [2]. Unlike mass and stiffness systems, the understanding of damping is considerably less comprehensive, making it challenging to predict vibration parameters for damping in practice [3]. Rayleigh damping, characterized by predefined constants α and β are, provides an approximate approach but is limited to global damping representation rather than individual element behavior. While effective in large-scale simulations, it does not offer a clear physical interpretation, making it insufficient for discrete one-dimensional elements such as springs and dampers.

Despite various studies exploring damping in single and multi-degree-of-freedom systems, most approaches focus on modal damping ratios or empirical tuning rather than a direct measurement-based methodology. Moreover, widely used damping models in FEM simulations are predominantly suited for large-scale systems rather than individual discrete elements. Our study addresses this gap by providing a direct, efficient method to obtain a damping coefficient in SI units, ensuring realistic simulation behavior in FEM software such as LS-DYNA but it is also applicable to any FEM system

Review of existing damping estimation methods: limitations and the need for a novel approach

General problem of viscous damping and evaluated MEMS accelerometers for damping identification but there is a lack of the direct designation of the damping coefficient. The work [4] presents an experimental performance evaluation of six low-cost MEMS accelerometers for identifying natural frequencies and damping ratios of a three-storey frame model and a reinforced concrete slab and their noise characteristics. The results showed an overall good performance of the MEMS accelerometers, but with identified natural frequencies only (Fig. 1).

In the [5] a novel method of identification of the coefficients of the damped parametric oscillator. The method is dedicated to periodic signals and relatively complicated laboratory set up. The authors focus on the difficulty of analyzing real sliding and rolling frictional contact pairs, such as those in bearings. In their methodology, they do not independently determine the damping coefficient but rather adjust it to achieve agreement between numerical results and experimental data. The main objective of their work is to analyze the system's behavior and identify parameters influencing its dynamics, rather than independently determining the damping coefficient (Fig. 2).

In [6], similar numerical results obtained through continuation and collocation methods were successfully compared to experimental results on nonlinear vibrations of a rectangular stainless steel plate. However, the damping coefficient was provided as a damping ratio rather than a real value, making the solution difficult to apply in practice. Moreover, the damping coefficient was adjusted for a long time until it matched the experiment, meaning that damping was not determined directly but rather adjusted.

The authors of paper [7] focused on the design and identification of parameters of a tuned

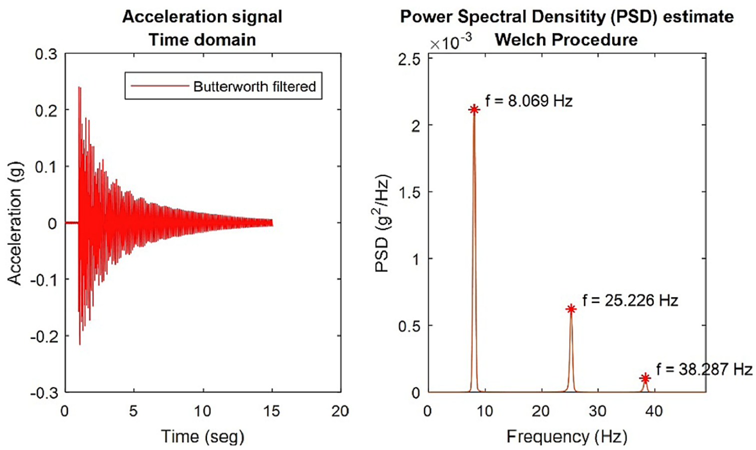

Figure 1. Time domain and PSD with Peak-Picking results plot (SHM equipment test) [4]

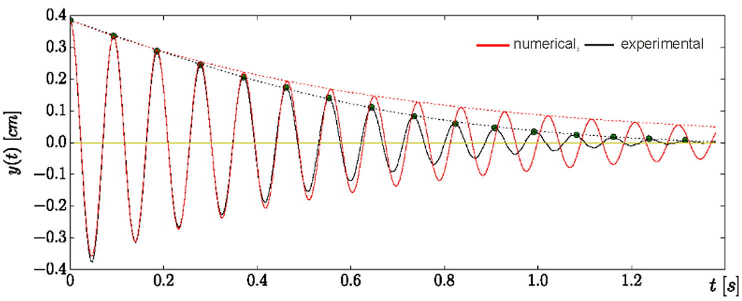

Figure 2. Comparison of two-time histories confirming discrepancy between the experimental trajectory, and correspondingly, the analytical exact solution [5]

mass damper (TMD) with an inverter. They conducted experimental studies to validate their model and analyzed energy dissipation mechanisms, including viscous and Coulomb damping. Regarding the damping coefficient, they did not independently determine it from first principles or experimental measurements alone. Instead, they followed a two-step procedure to identify the damping coefficients, starting with an analytical estimation and then refining the values through numerical fitting to experimental data. This means they adjusted the damping coefficients to match their experimental results, rather than deriving them purely from theoretical calculations or direct independent measurements. To validate the model they compare the numerical and experimental time traces. Good matching of the results prove well-posedness of the model and confirm the obtained parameters values (Fig. 3).

In [8] the authors investigated the role of Rayleigh damping only in the nonlinear numerical seismic analysis of tunnels. They focused on how different approaches to selecting damping parameters influence tunnel response during earthquakes. Their study was based on numerical simulations using a two-dimensional finite difference model (FLAC), incorporating the Mohr-Coulomb failure criterion for soil behavior. Regarding the damping coefficient, the authors did not independently determine it based on direct measurements or theoretical derivation. Instead, they analyzed different empirical approaches for selecting Rayleigh damping parameters. They examined how the choice of target damping ratio (ξ_{tar}) (Fig. 4)

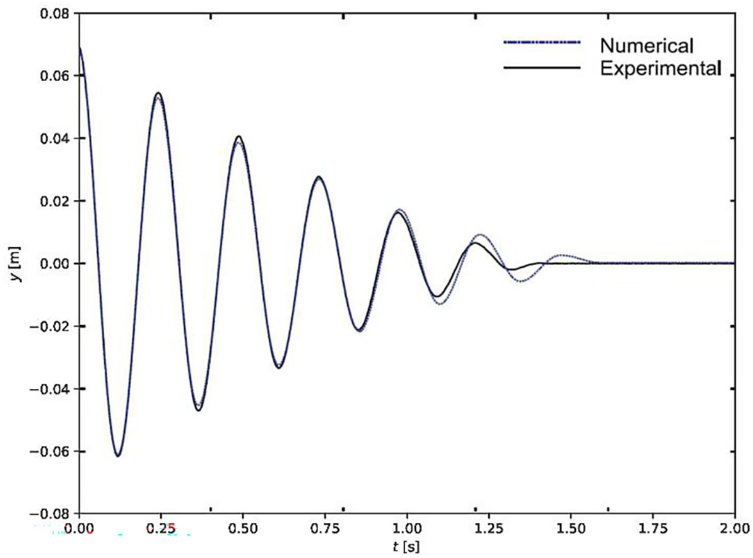

Figure 3. Comparison of the experimentally and numerically obtained time traces of free vibrations of the main oscillator with the classical tuned mass dampers and the continuously variable transmission [6]

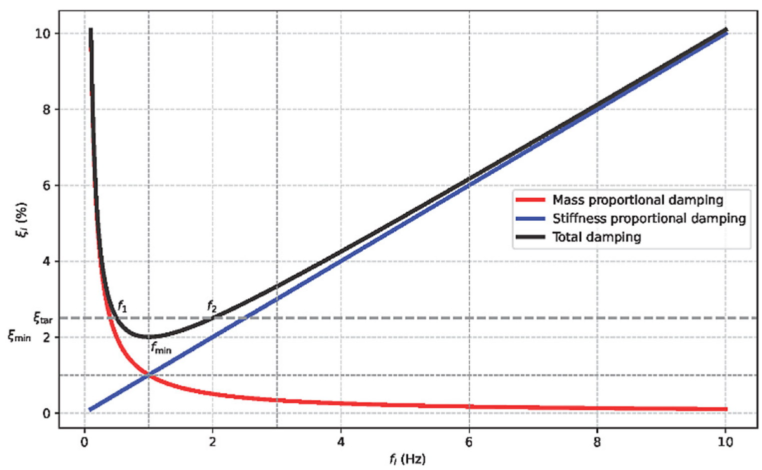

Figure 4. Rayleigh damping as a function of frequency [8]

and the frequency range for Rayleigh damping influenced numerical results. The damping values were not uniquely identified but rather chosen based on common engineering assumptions and guidelines from previous studies.

In [9] the authors present results from tests on typical shock absorber designs using various rubber and elastomer types. The studies, conducted on a tensile testing machine, assessed static and dynamic stiffness, while a lightweight drop hammer measured the damping coefficient characteristics under high-speed wave interactions, specifically the Shock Response Spectrum (SRS). Additionally, the research included rheological analysis on the impact of harmonic vibrations on stiffness and damping coefficients in shock absorber materials, although damping coefficients were not directly determined.

Many authors have studied the problems arising from the use (or misuse) of Rayleigh damping [3, 10, 11]. The use of the proportional stiffness part of the damping based on the original ambiguous damping forces may result in overestimated designs and a lack of static equilibrium. Various models are used to address this issue [12–14]. Consequently, many researchers have shifted to experiment-based fitting methods (Fig. 5) [15, 16] to determine the damping properties. Estimating damping in a structure composed of different materials and processes remains one of the most difficult challenges (Fig. 6a) [17]. Typically, the determination of the damping ratio requires sophisticated laboratory equipment, gauges, and stationary measurements (Fig. 6b) [18]. The authors of the paper recommend a novel approach using a low-cost MEMS accelerometer and a Python-based algorithm to directly measure damping coefficients in SI units, providing an alternative to existing experimental and numerical estimation methods.

METHODOLOGY OF DAMPING COEFFICIENT DETERMINATION

The primary challenge in this study is determining the damping coefficient based on

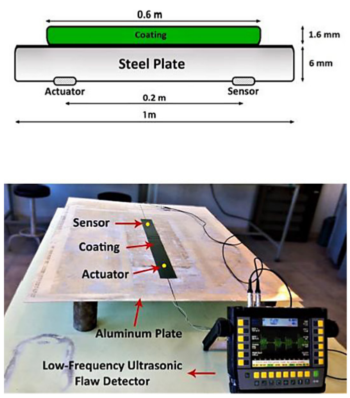

(a)

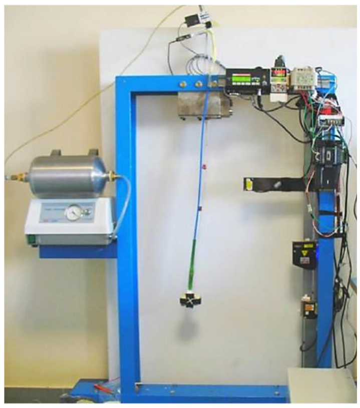

(b)

Figure 5. Experimental setups: (a) ultrasonic flaw detector DIO-1000 STARMANS next to the aluminum coated plate [15] (b) the layered beam with the granular damping element marked with X [16]

(a)

(b)

Figure 6. Experimental setups: (a) the layered beam with the granular damping element marked with X [17] (b) ultrasonic flaw detector DIO-1000 STARMANS next to the aluminum coated plate [18]

displacement data derived from acceleration measurements. The conventional approach involves double integration of acceleration signals to obtain displacement; however, this method introduces drift and significant errors. Standard solutions do not provide a straightforward way to correct this issue. In this work, we address this problem by implementing advanced filtering techniques in Python, which are widely available and accessible, making this solution novel compared to existing industrial applications.

Acceleration measurement and accuracy considerations

Accelerometers are the most commonly used transducers for measuring the vibration responses of structures. There are many methods for extracting the parameters of a measured signal described in the literature, ranging from classical Fourier transformation methods [19–21] to state-of-the-art ones [22–25]. Some relatively simple attempts have been made to determine the damping ratio by measuring displacement as a low-cost 'plug-and-play' method. The solutions described in [26] are the easiest and the cheapest ones, but they are a little hard to use as a mobile set and have relatively low accuracy.

The common experimental method of determining the damping coefficient using MEMS starts from the reconstruction of the displacement signal by taking the inverse Fourier transform of the magnitude of the significant frequency components of the Fourier transform of the acceleration signal [27]. However, reconstructing low-frequency signals in the frequency domain will produce biased errors [28].

The authors chose the double integration of the time domain's acceleration signal as the method for determining the damping coefficient. This method has also a serious drawback, in that there is a high amount of zero-shift and drift [29] but it is intuitive and fast if the mentioned obstacles were removed, which was solved using Python software and presented in the paper. To perform the verification of the obtained results, the well-known data of a spring (Fig. 7a) were chosen. The authors intended to make the measuring station (Fig. 7b) as simple as possible so that the results obtained could be easily replicated without complicated apparatus.

Observing the simplicity of the measurement setup, including the phone mounting and consequently the accelerometer placement, one might question the professionalism and repeatability of the results. However, this setup was intentionally

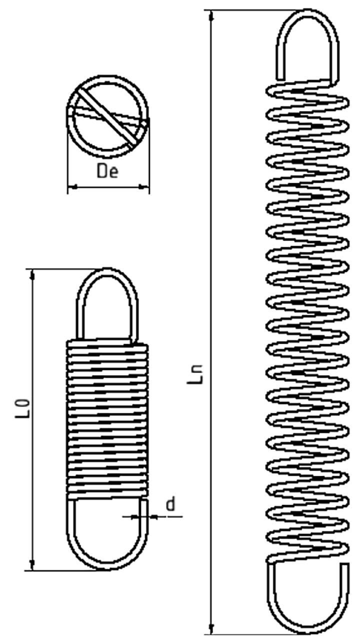

(a)

(b)

Figure 7. The data of spring: (a) spring's parameters: d = 1.91 mm, L_0 = 76.20 mm, D_e = 21.59 mm, L_n = 161.54 mm, F_n = 81.85 N–maximum allowable load at Ln, (b) simple measuring station with the mass of the weight m = 5.3 kg and the initial deflection u_0 = 4 cm

designed to demonstrate both the simplicity and effectiveness of the proposed solution. The strength of this approach lies in showing that complex apparatus is not always necessary.

Multiple repeated trials have confirmed that the mounting method does not significantly affect the results, which remain consistent and reproducible. This is easily verifiable through repeated measurements. In contrast, performing the same task with a more complex system would introduce additional variability and dependencies. The key factor is not how the system is mounted, but rather how the accelerometer captures displacement data, as the sought damping coefficient is embedded in this displacement. The crucial step is extracting this value accurately, which has been successfully achieved in this study.

The acceleration was recorded within 10 seconds (Fig. 8–10) with a sampling frequency of f_{sample} = 500 Hz (dt = 0.002 s). The recording was performed using a MEMS accelerometer, which is available on any mobile phone, with the freely available application Resonance [30] or Phyphox [31]. Applications like Resonance (and many others) generally record only acceleration and are not capable of calculating a specific value for the damping. The authors want to emphasize that the procedure for determining the damping coefficient can be available with ordinary equipment, which is also the outcome of the paper.

Figure 8 shows the recorded acceleration signal. The acceleration signal from Figure 8 was then integrated to obtain the velocity Figure 9. Finally, the velocity signal was integrated to obtain the displacement vs. time plot of the vibrating system (Fig. 10).

It was expected that the simple procedure of integrating the acceleration and velocity signals to obtain the displacement waveform over time would lead to a determining envelope of the signal. Then the damping coefficient, however in practice was not possible to do in the first stage (Fig. 10). If there is nothing suspicious at first glance in Figure 8 and Figure 9, then in Figure 10, we can see that integrating the previous signals leads to a displacement that takes almost half a meter in 10 seconds, which is nonsensical. As stated in [29], the phenomenon shown in Figure 11 is referred to as "drift", and it is primarily caused by friction and elasticity in the sliding guide. To confirm that the

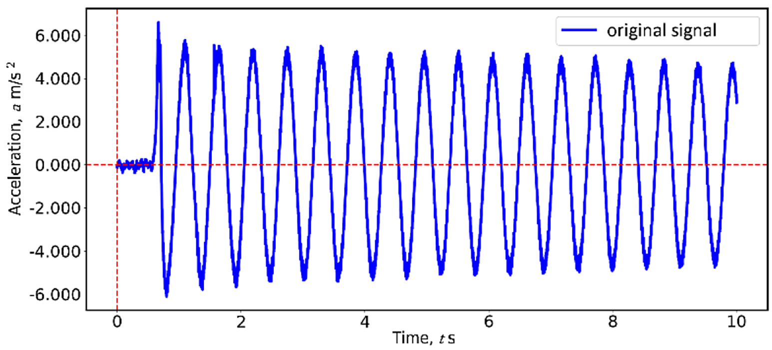

Figure 8. Acceleration: m = 5.3 kg, u_0 = 4 cm, f_{sample} = 500 Hz, dt = 0.002 s; acceleration due to gravity was intentionally excluded from the measurement

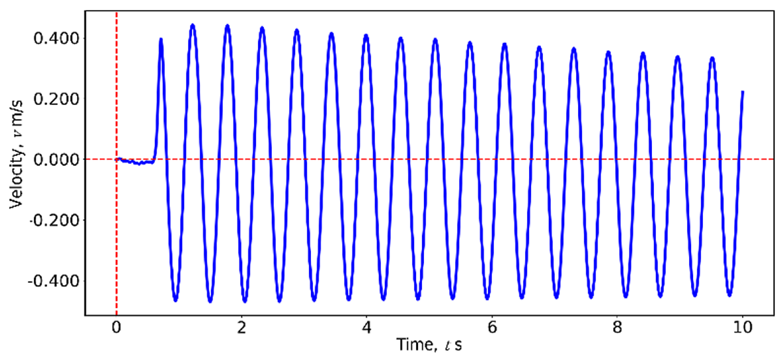

Figure 9. Velocity as the integral of acceleration from Fig. 8

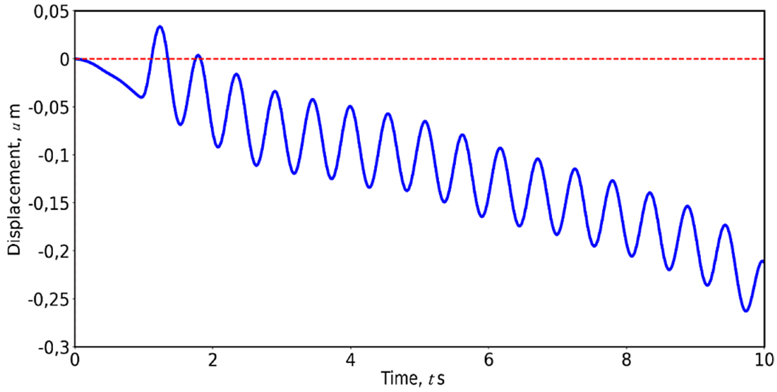

Figure 10. Displacement as double integral of velocity from Fig. 9

signal distortion was caused by "drift", the measurements were repeated and recording time was extended to t = 60 s (Fig. 12–14). During the new measurements, drift was observed again, revealing the same distortion in displacement as observed previously (compare Fig. 10 and Fig. 14).

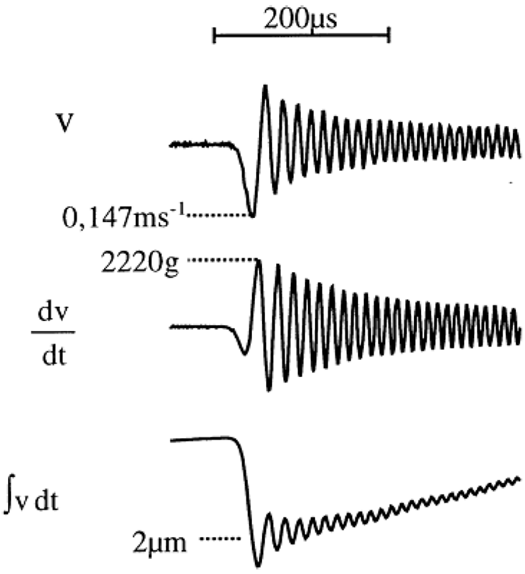

Figure 11. Drift because of friction and elasticity in the sliding guide according to [29]

Above steps revealed that "drift" is caused by integration constants that needed to be removed. This is the main obstacle in directly determining the damping coefficient from acceleration measurements, as documented in the literature [29], but no methods for overcoming this problem are provided. With knowledge of signal processing, procedures available in Python can be applied to extract displacement signals by filtering out noise. This approach has not been found in the scientific literature and constitutes a novel aspect of this study.

Acceleration signal filtering

The main frequencies are most conveniently represented in the frequency domain. Figure 15 displays the acceleration spectral amplitude on a linear scale, while Figure 16 represents the same amplitude in decibel scale. The notable frequency is 1.72 Hz, corresponding to the spring oscillation frequency. For illustration, the sought frequency is shown alongside the frequency of gravitational

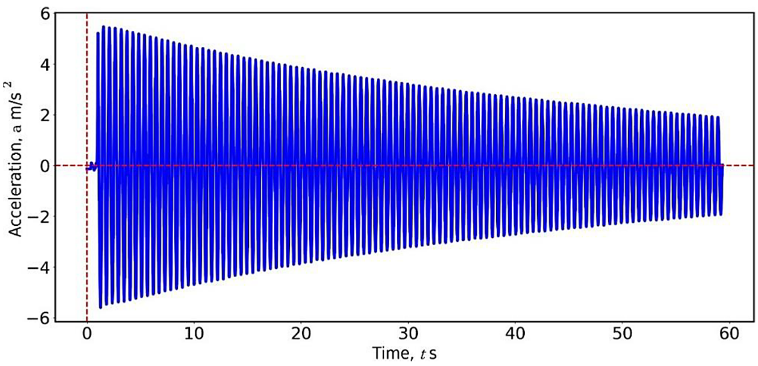

Figure 12. Acceleration: m = 5.3 kg, u_0 = 4 cm, f_{sample}=500 Hz, dt = 0.002 s

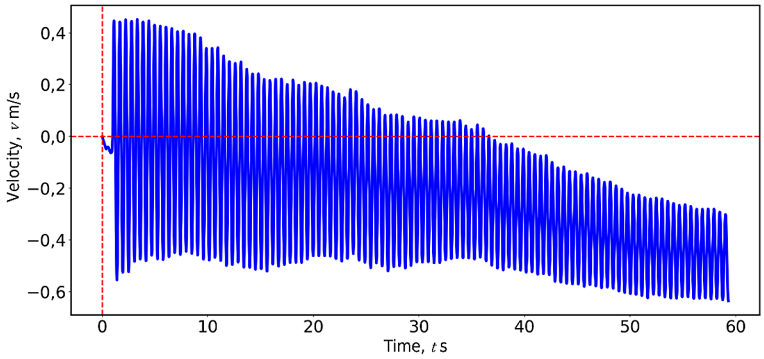

Figure 13. Velocity from integration of acceleration data

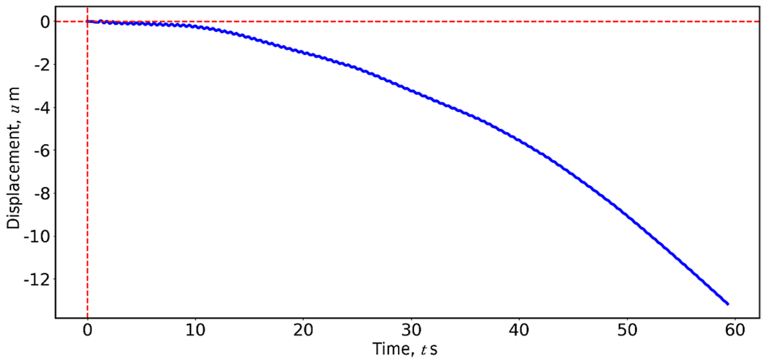

Figure 14. Displacement from integration of velocity data

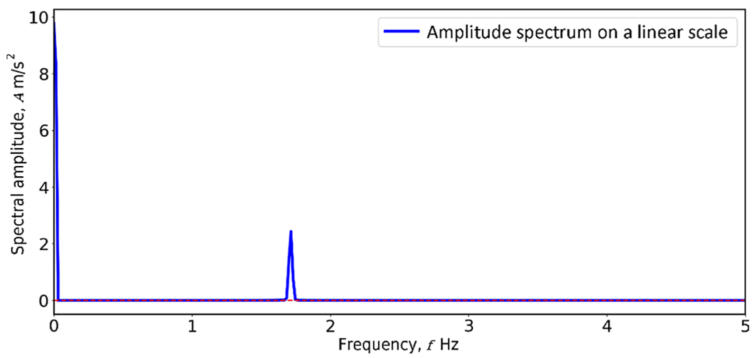

Figure 15. Acceleration spectral amplitude on the linear scale

acceleration g, which is not relevant in this context. It can be filtered out using the same methodology as a constant component or excluded at the acceleration measurement stage. In this study, the latter approach was applied from the beginning of the measurements. Filters, as depicted in Figure 17, were applied to remove the effects of drift and the integration constant, to isolate the dominant frequency. Figure 18 presents both a simplified and a detailed version of the algorithm for damping ratio determination. After extracting the frequency of 1.72 Hz, the data can be presented on the decibel scale (Fig. 19), which reveals the removal of all distortions derived from the MEMS accelerometer (Fig. 16). Multiple filters were tested, and the most effective one was chosen, represented by the blue line ultimately (butter irr 20), a clear signal was obtained (Fig. 19) without drift error. An envelope could be created (Fig. 20) which is needed to determine the damping coefficient. Finally damping factor obtained by the implementation the algorithm from Figure 18, was c ≈ 0.2 ≈ $\frac{N}{m}s$. The

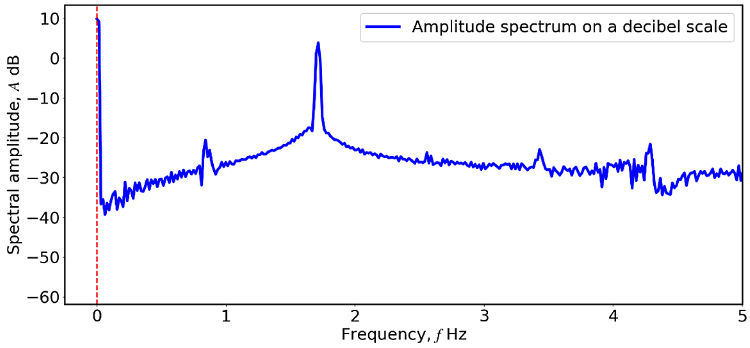

Figure 16. Acceleration spectral amplitude (Fig. 16) in decibel scale

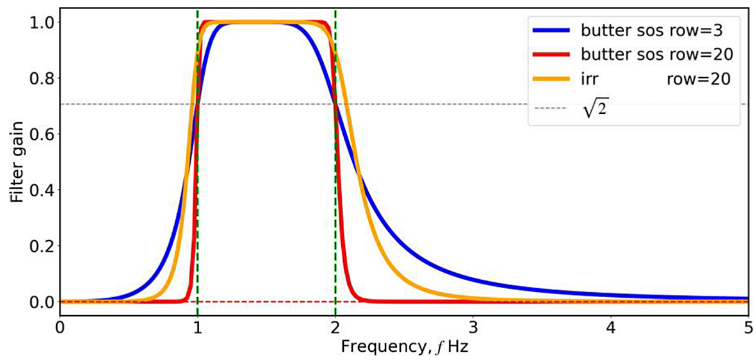

Figure 17. Characteristics of bandpass filters 1 Hz to 2 Hz

source codes in the papers are always problematic and limited in terms of editing. Nevertheless, they have been graphically presented in both a simple and a detailed version. The detailed version should be readable for IPython users, who should easily take advantage of it and find the relevant issues of interest. If this is not the case, upon request in the editor board or directly from [35], the code is available for review. Before running it, users should configure their own Jupyter environment with the required libraries.

Analytical and numerical verification of the determined damping coefficient

Points through which the envelope passes (Fig. 20) were approximated by the function

$$u(t) = e^{-pt} K \sin(qt) \tag{2}$$

where: $K = u_{a0_{(t=0)}} = 40$ mm is the initial spring deflection, $q = \sqrt{\left(\frac{c}{2m}\right)^2 - \frac{k}{m}}$, c, c – damping coefficient, m – mass, k – elasticity coefficient of the material. To determine the damping coefficient c the following relationships were used $p = \frac{c}{2m}$, so

$$c = p \cdot 2m \tag{3}$$

Beforehand, the parameter p must be calculated using a logarithmic position u (linearization), i.e. a straight line fit

$$u(t) = e^{-pt} \text{ then } -p = \frac{1}{t}\ln(u(t)) \tag{4}$$

Then the damping factor, determined for the case under consideration, is:

$$c = -p \cdot 2m =$$
$$= -(-0.0179) \cdot 5.3 = 0.1897 \approx 0.2 \, \frac{N}{m} s$$

To verify the obtained damping factor c, the calculations were repeated using independent measurements of the damping degree γ for the spring under consideration for $n = 97$, where n is the number of complete vibration cycles. In the case of harmonic damped oscillations, the value of both the decrement and logarithmic decrement is constant in time, therefore, to determine these parameters it is not necessary to know two consecutive amplitudes [32]. It is enough to know the amplitude a_n and the amplitudes of subsequent cycles (for cos qt = 1), which determines the equation

$$u_{a_n} = u_{a_0} e^{-pt} = u_{a_0} e^{-pnT} = u_{a_0} e^{-n\delta} \tag{5}$$

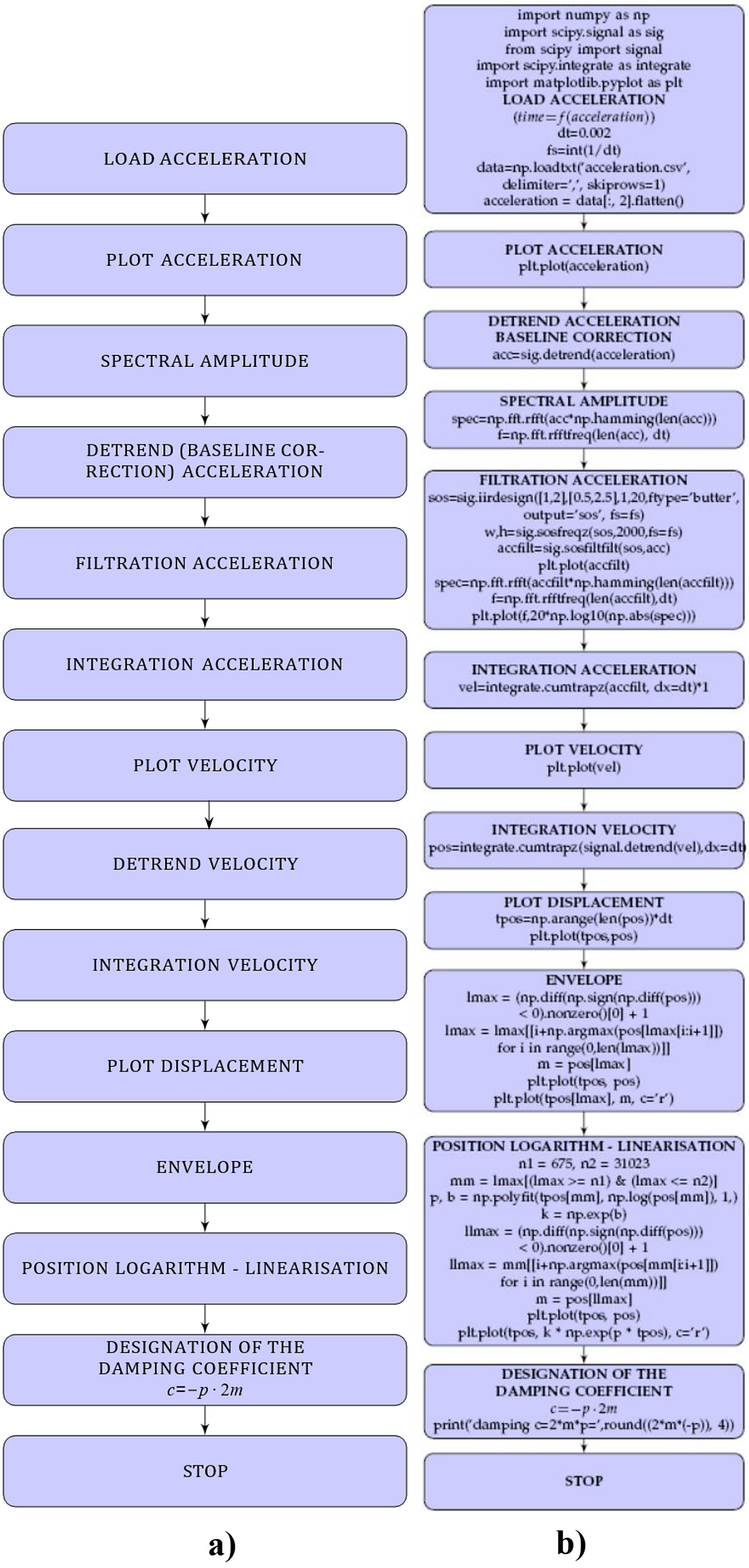

Figure 18. Python algorithm designation of damping ratio: (a) a simplified; (b) detailed version of the algorithm [35]

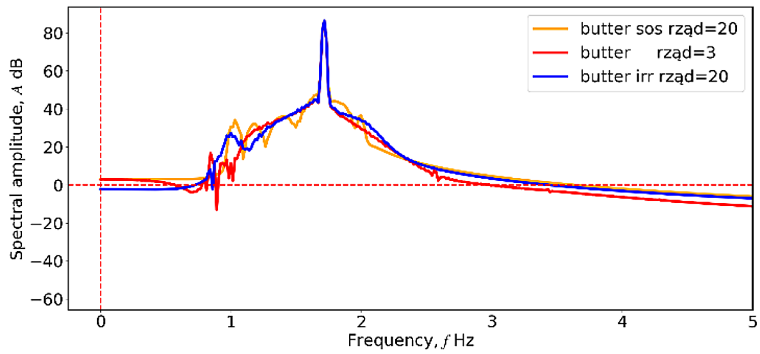

Figure 19. Acceleration spectral amplitude (Fig. 17) in decibel scale after filtration

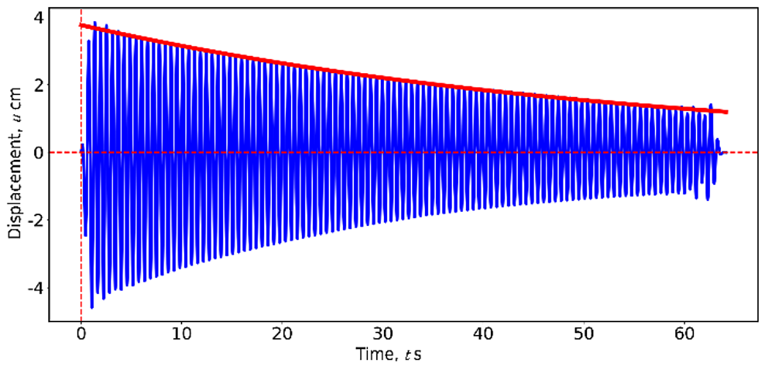

Figure 20. Displacement with envelope. Superimposition of the estimated envelope

From here we calculate

$$e^{-n\delta} = \frac{u_{a_n}}{u_{a_0}} \tag{6}$$

$$-n\delta = \ln \frac{u_{a_n}}{u_{a_0}} \tag{7}$$

$$\delta = -\frac{1}{n} \ln \frac{u_{a_n}}{u_{a_0}} \tag{8}$$

$$\delta = \frac{1}{n} \ln \frac{u_{a_0}}{u_{a_n}} \tag{9}$$

in this example n = 97, so

$$\delta = \frac{1}{n} \ln \frac{u_{a_0}}{u_{a_n}} = \frac{1}{97} \ln \frac{4}{0.679} = 0.0182827682 \tag{10}$$

because the logarithmic decrement of damping

$$\delta = pT = 2\pi \frac{p}{q} = \frac{2\pi\gamma}{\sqrt{1-\gamma^2}} \tag{11}$$

thereby

$$\delta^2 - \delta^2\gamma^2 = 4\pi^2\gamma^2 \tag{12}$$

then by transforming (14), to determine the degree of damping

$$\gamma = \frac{\delta}{\sqrt{4\pi^2 + \delta^2}} = \frac{1}{\sqrt{\left(\frac{2\pi}{\delta}\right)^2 + 1}} = \frac{1}{\sqrt{\left(\frac{2\pi}{0.0182827682}\right)^2 + 1}} = 0.0029097806 \tag{13}$$

using the formula

$$\gamma = \frac{c}{c_{kr}} \tag{14}$$

where: $ckr = 2\sqrt{km}$ – is the critical damping for the spring, the damping ratio can be determined as

$$c = \gamma \cdot 2\sqrt{km} = 0.0029097806 \cdot 2 \cdot \sqrt{676.169 \cdot 5.3} = 0.3798290195 \ \frac{N}{m}\mathrm{s} \tag{15}$$

The measurements were repeated to perform the final theoretical verification and validate the accuracy of the determined damping factor using the MEMS accelerometer. The spring vibrations were recorded using the slow-motion option under the same conditions and the time between amplitudes was measured. The logarithmic decrement of damping, $\delta = pT = ln\frac{u_n}{u_{an}+1}$, was calculated using the recorded amplitude values and the corresponding time intervals, allowing the determination of the damping coefficient, *c*. Using the relationship in (7).

$$e^{-pt} = \frac{u_a(t)}{u_{a_0}} \tag{16}$$

$$-pt = \ln\frac{u_a(t)}{u_{a_0}} \tag{17}$$

assuming that $p = \frac{c}{2m}$ we get the result

$$-\frac{c}{2m}t = \ln\frac{u_a(t)}{u_{a_0}} \tag{18}$$

$$\frac{c}{2m} = -\frac{1}{t}\ln\frac{u_a(t)}{u_{a_0}} \tag{19}$$

$$\frac{c}{2m} = -\frac{1}{t}\ln\frac{u_{a_0}}{u_a(t)} \tag{20}$$

$$c = \frac{2m}{t}ln\frac{u_{a0}}{u_a(t)} = \frac{2\cdot 5.3}{4.98}\cdot ln\frac{3.3}{2.9} = \\ = 2.128\cdot 0.1292 = 0.27\frac{N}{m}s \tag{21}$$

In conclusion, rounding the MEMS result of the damping factor to $0.1897 \approx 0.2\,\frac{\mathrm{N}}{\mathrm{m}}\mathrm{s}$ and comparing it with the value obtained from an accurate 'slow motion' measurement of $0.27\frac{\mathrm{N}}{\mathrm{m}}\mathrm{s}$, it is evident that the results are correct. The damping factor has been numerically designated (Fig. 21) and verified with the equation of motion (Equation 22) which has been solved using the standard explicit algorithm Euler method according to the algorithm (Fig. 19) both using an independent program written in Python and corresponding to the experiment with given parameters (Fig. 7)

$$\frac{d^2u}{dt^2} + \frac{c}{m}\frac{du}{dt} + \frac{k}{m}u = F(t) \tag{22}$$

where: $F(t)$ – is a forcing force. The results are correct.

Finally, simulations of the operation of the spring under consideration were carried out using a discrete elastic element with damping (Fig. 22) in LS-Dyna [35]. The numerical simulation of the spring-mass system with damping was conducted in LS-Dyna using a discrete element approach. The system was modeled with an *ELEMENT_DISCRETE definition, where the mass m = 5.3 kg was assigned using the *ELEMENT_MASS card, and the elastic and damping properties were implemented via *MAT_SPRING_ELASTIC and *MAT_DAMPER_VISCOUS, respectively. The stiffness coefficient was set to k = 676.2 N/mk, and the damping coefficient was initially chosen as c = 0.2 Ns/m. The gravitational load was applied using the *LOAD_BODY_Y function. In the LS-DYNA model, there is no need for a separate implementation of preload due to gravity, as gravitational forces are automatically considered in the dynamic analysis. Additionally, the interaction between bodies, including friction and the influence of the air medium, was not required for the objectives of the simulation.

The simulation was carried out for t = 60 s during which the displacement of the mass was recorded. Initial conditions were imposed by prescribing an initial displacement of u_0 = 4 cm. The results were compared with analytical solutions and experimental data, confirming the correctness of the damping coefficient and overall model behavior.

If the damping coefficient had been designated properly, the simulated vibration would have behaved in the same way as in the real experiment and theoretical computation (Fig. 21), especially from the damping point of view. Figure 23 shows the confirmation that the damping coefficient was determined correctly, all of the signals match, which means that the methodology is satisfied. For the graph (Fig. 23) an error analysis

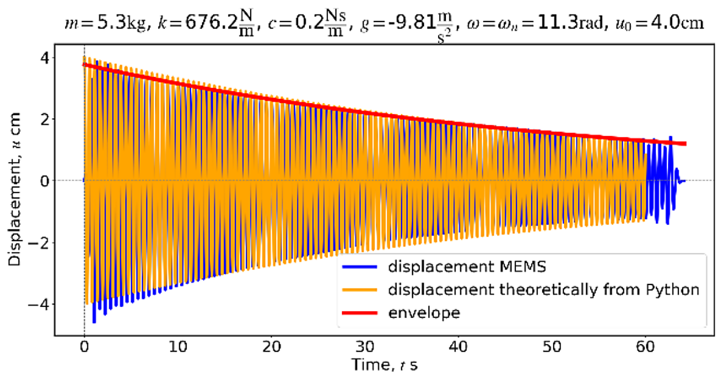

Figure 21. Verification of the determined damping factor with an in-house program; initial displacement u_0 = 4 cm

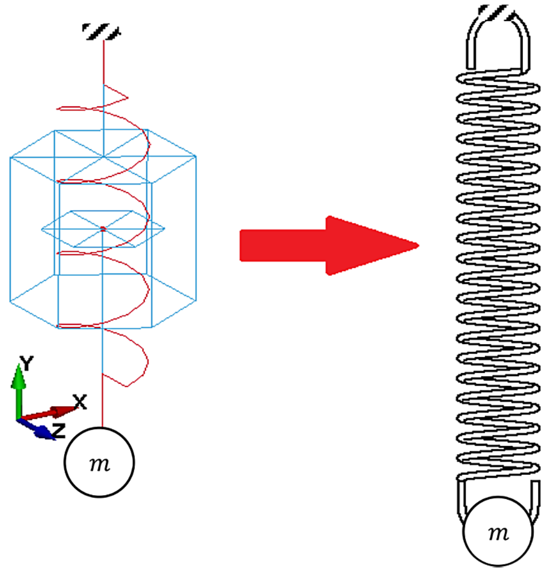

Figure 22. Representation of FEM discrete element as the spring with damping

100% accuracy is not the goal from the FEM perspective. For the FEM simulation itself, the obtained damping coefficient provides satisfactory results and physically represents the damping element, which is a qualitative advantage. This is particularly relevant because, in general, FEM simulations are performed without damping.

The make sure that the FEM simulation was carried out correctly, the damping coefficient was increased from c = 0.2 to c = 71.83 Ns/m as 60% of the critical spring damping $ckr = 2 \cdot \sqrt{k \cdot m} = 119.73$ Ns/m and the results were compared with the theoretical one (Fig. 25). The results were satisfactory. Several additional steps were taken to ensure the correctness of the simulation. In this instance (Fig. 26), the damping ratio was increased from 0.2 Ns/m to 5.2 was performed to assess the fit between MEMS displacement measurements and LS-DYNA simulation results using MAE (Mean Absolute Error $1/n \sum_i |y_i - \hat{y}_n|$) and MSE (Mean Square Error $1/n \sum (y_i - \hat{y}_n)^2$). The obtained results were MAE=1.84 i MSE=5.56 (Fig. 24). The red line represents the ideal fit ($y = x$), while the black line shows the actual relationship between MEMS and LS-DYNA results. High MAE and MSE values indicate significant deviations, suggesting the need for further calibration or filtering. However, from the FEM simulation perspective, this evaluation method may not be well suited, as it naturally results in high MAE and MSE values.

This indicates that future work should focus on refining the filtering method, but achieving

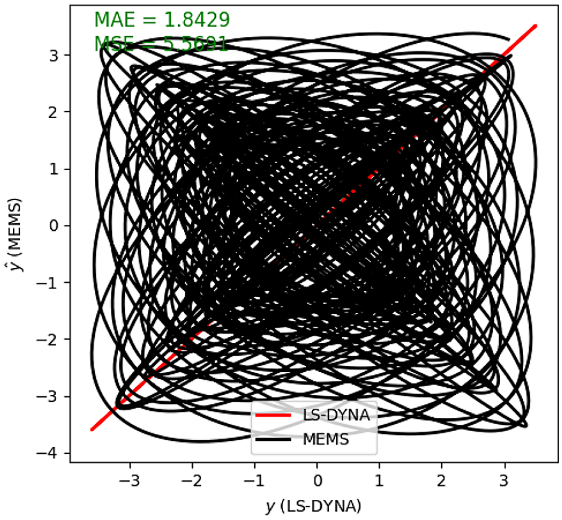

Figure 24. Comparison of MEMS displacement measurements with LS-DYNA simulation results using MAE and MSE regression metrics

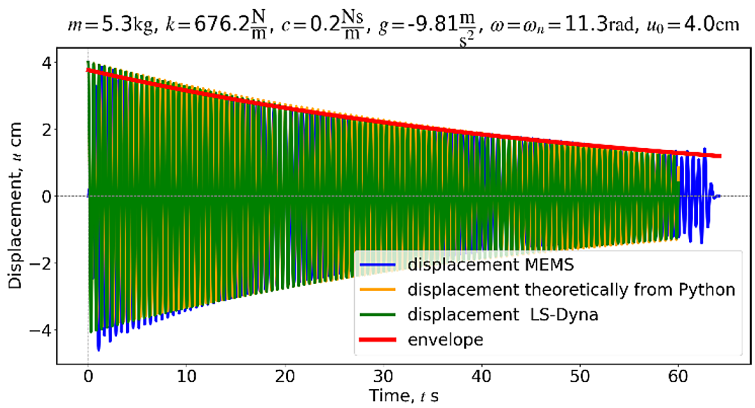

Figure 23. Comparison of the influence of the spring rate and damping on the results obtained using the MEMS signal, the proprietary Python program, and the LS-Dyna

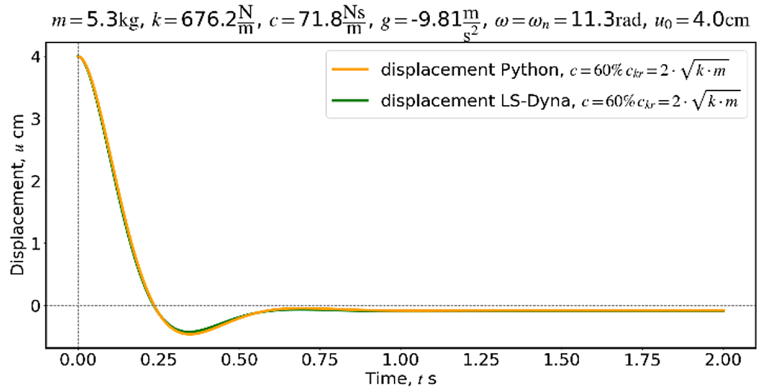

Figure 25. Comparison of the vibration waveform with the critical spring damping for a discrete elastic element with damping modeled in Python

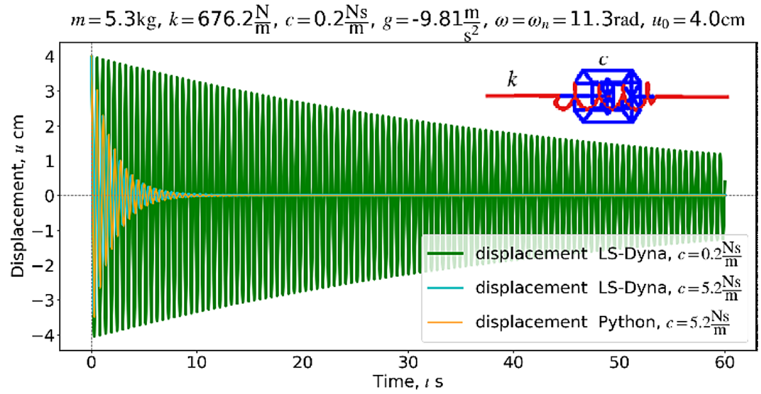

Figure 26. Vibration waveform for the discrete elastic element with damping modeled in LS-DYNA c = 0.2 Ns/m compared with the simulation for c = 5.2 Ns/m and the theoretical one from Python

Ns/m, and the results were compared with those obtained in Python. To provide a basis for comparison, the simulation results for c = 0.2 Ns/m are also shown in the background. Figure 26 illustrates a well-established phenomenon and confirms the accuracy of the simulations.

Upon analyzing the initial signal, it became evident that the first amplitude remained relatively constant in both cases, with the stiffness coefficient being primarily responsible for this behavior. On the other hand, the damping ratio governs the damper's performance during the remaining period, offering insights into the duration of damper movement or the speed of damping.

In conclusion, relying solely on the stiffness coefficient to evaluate dampers provides information about their rigidity and impact amplitude, but it falls short of assessing their behavior over time. This study contributes to a more comprehensive understanding of damper modelling in FEM simulations by introducing the damping coefficient and the method outlined in this paper. The method presented here can be applied to any spring-damper element where a periodic signal is observed.

CONCLUSIONS

The outlined method presents a novel approach to determining the damping coefficient using a MEMS accelerometer, particularly for FEM simulations discrete elements where damping is required. The primary innovation lies in its ability to determine the damping coefficient in SI units directly from acceleration data, without requiring complex and costly laboratory setups or arbitrary empirical adjustments. The algorithm effectively reconstructs displacement data while addressing issues such as drift and noise interference, which are common limitations in conventional double-integration approaches.

The question arises as to whether the proposed method can be extended to any arbitrary signal. In general, the answer is affirmative, as preliminary tests have yielded promising initial results. First positive results have been obtained; however, at this stage, they have been resigned from the article as they require further research and diverging from its primary focus. However, further research and refinements, particularly in signal filtering, are necessary. At this stage, the method has been validated for periodic signals typical of springs, dampers, and other structured attenuators.

Future work will focus on extending the methodology to more complex signals by incorporating advanced mathematical and numerical techniques, particularly in filtering and signal identification. Future iterations of the algorithm will integrate enhanced data processing techniques to mitigate interference from non-periodic components. Refining filtering methods and signal extraction will be crucial in improving the algorithm's capability to isolate relevant data in complex, multi-frequency environments. Analyzing the noise spectrum across accelerometer axes will aid in designing a high-pass filter to suppress low-frequency noise, while applying an inverse Fourier transform will further refine acceleration data and minimize interference. As the approach continues to evolve, it presents a valuable alternative to traditional damping coefficient determination methods, offering enhanced physical realism and broad applicability in structural dynamics, vibration analysis, and mechanical system optimization.

Computations were carried out using the computers of Centre of Informatics Tricity Academic Supercomputer & Network.

REFERENCES

1. https://tiny.pl/9n68m 1998–2023: acces on 2022-03-21.
2. Chowdhury I, Dasgupta S. Computation of Rayleigh damping coefficients for large systems. The Electronic journal of Geotechnical Engineer 2003; 43(6855–6868): 1–11.
3. Liu M, Gorman D.G. Formulation of Rayleigh damping and its extensions. Computers & Structures 1995; 57(2): 277–285.
4. Ribeiro R.R, Lameiras R. Evaluation of low-cost MEMS accelerometers for SHM: Frequency and damping identification of civil structures. Latin American Journal of Solids and Structures 2019: 16(7): 203.
5. Olejnik P, Awrejcewicz J. Coupled oscillators in identification of nonlinear damping of a real parametric pendulum. Mechanical Systems and Signal Processing 2018; 98: 91–107.
6. Amabili M. Nonlinear damping in nonlinear vibrations of rectangular plates: Derivation from viscoelasticity and experimental validation. Journal of the Mechanics and Physics of Solids 2018; 118: 275–292.
7. Lazarek M, Brzeski P, Perlikowski P. Design and identification of parameters of tuned mass damper with inerter which enables changes of inertance. Mechanism and Machine Theory 2018; 119:C: 161–173.
8. Sun Q, Dias D. Significance of Rayleigh damping in nonlinear numerical seismic analysis of tunnels. Soil Dynamics and Earthquake Engineering 2018; 115: 489–494.
9. Grządziela A, Kluczyk M. Shock absorbers damping characteristics by lightweight drop hammer test for naval machines. Materials 2021; 4(14): 772.
10. Hall J. F. Problems encountered from the use (or misuse) of Rayleigh damping. Earthquake Engineering & Structural Dynamics 2006; 35(5): 525–545.
11. Mohammad D, Khan N, Ramamurti V. On the role of Rayleigh damping. Journal of Sound and Vibration 1995; 185(2): 207–218.
12. Alipour A, Zareian, F. Study Rayleigh damping in structures; uncertainties and treatments. The 14th world conference on earthquake engineering 2022; 12–17.
13. Tian Y, Fei Y, Huang Y, Lu X, A. Universal rate-dependent damping model for arbitrary d a m p - ing- frequency distribution. Engineering Structures 2021; 255: 113–894.
14. Rahul B, Dharani J, Balaji R. Optimal method for determination of rayleigh damping coefficients for different materials using modal analysis. International Journal of Vehicle Structures & Systems 2021; 13(1): 102–111.
15. Mehrabi M, Soorgee M.H, Habibi H, Kappatos V. An experimental technique for evaluating viscoelastic damping using ultrasonic guided waves. Ultrasonics 2022; 123: 106–707.
16. Bajkowski J.M, Dyniewicz B, Bajer C. I. Damping properties of a beam with vacuum-packed granular damper. Journal of Sound and Vibration 2015; 341: 74–85.
17. Mevada H, Patel D. Experimental Determination of Structural Damping of Different Materials. Procedia Engineering 2016; 144: 110–115.
18. Shirzadeh R, Devriendt C, Bidakhvidi M.A, Guillaume P. Experimental and computational damping estimation of an offshore wind turbine on a monopile foundation. Journal of Wind Engineering and Industrial Aerodynamics 2013; 120: 96–106.
19. Bendat J.S, Piersol A.G. Random data: Analysis and Measurement Procedures 2011: John Wiley & Sons.
20. Newland D.E. Random vibrations, spectral & wavelet analysis. Longman Scientific & Technical. 1993; 5.

21. Papoulis A, Pillai S.U. Probability, random variables, and stochastic processes 2002: Fourth Edition McGraw-Hill New York.
22. Chen Z, Mechefske, C.K. Machine signature identification by analysis of impulse vibration signals. Journal of Sound Vibration 2001; 244(1): 155–167.
23. Lee S.K. Application of the L-Wigner distribution to the diagnosis of local defects of gear tooth. KSME International Journal 1999; 13: 144–157.
24. Luo G.Y, Osypiw D, Irle M. Real-time condition monitoring by significant and natural frequencies analysis of vibration signal with wavelet filter and autocorrelation enhancement. Journal of Sound and Vibration: 2000; 236(3): 413–430.
25. Tang S.K. On the time–frequency analysis of signals that decay exponentially with time.Journal of Sound and Vibration: 2000; 234(2): 241–258.
26. Varanis M, Silva A.L, Brunetto P.H.A, Gregolin R.F. Instrumentation for mechanical vibrations analysis in the time domain and frequency domain using the Arduino platform. Revista Brasileira de Ensino de Física 2016; 38(1): 5.
27. https://tiny.pl/7v18k Exploring Data Acquisition and Trajectory Tracking with Android Devices and Python 2019: acces on 2022-03-21.
28. Han S. Measuring displacement signal with an accelerometer. Journal of Mechanical Science and Technology 2010; 24(6): 1329–1335.
29. Knapp J, Altmann E, Niemann J, Werner K.-D. Measurement of shock events by means of strain gauges and accelerometers. Measurement: 1998; 24(2): 87–96.
30. https://tiny.pl/9nzgf Resonance-Vibration Analysis: access on 2022-03-21.
31. https://tiny.pl/wwxmx Phyphox App: acces on 2023-11-22.
32. https://tiny.pl/7vx96 Logarithmic damping decrement: access on 2023-11-22.
33. https://tiny.pl/wwxx6 Scipy Signal Iirdesign: access on 2023-11-22.
34. https://tiny.pl/wwxxb Scipy Signal Butter: access on 2023-11-22.
35. https://tiny.pl/dr8kby64 IPython and LS-Dyna source codes 2025-02-12